BIBECHANA
Vol. 20, No. 3, December 2023, 275-284

ISSN 2091-0762 (Print), 2382-5340 (Online)
Journal homepage: http://nepjol.info/index.php/BIBECHANA
Publisher:Dept. of Phys., Mahendra Morang A. M. Campus (Tribhuvan University)Biratnagar

Cr^{3+} substitution effect on Co-Cu and Cu-Co nano ferrites on structural and morphological properties

D. Parajuli[1,*], **N. Murali**[2], **K. Samatha**[3]

[1]*Research Center for Applied Science and Technology, Tribhuvan University, Kirtipur*
[2]*Department of Engineering Physics, AUCE (A), Andhra University, Visakhapatnam, India*
[3]*Department of Physics, AUCST, Andhra University, Visakhapatnam, India*

*Corresponding author. Email: deepenparaj@gmail.com

Abstract

The Cr^{3+} substituted Co-Cu ($Co_{0.7}Cu_{0.3}Fe_{2-x}Cr_xO_4$) and Cu-Co ($Cu_{0.7}Co_{0.3}Fe_{2-x}Cr_xO_4$) where x = 0.0, 0.05, 0.1, 0.15, 0.2 and 0.25 nanoferrite composite were prepared with the sol-gel approach. Their structural, DC electrical resistivity and magnetic properties were analyzed. XRD shows the single-phase spinel ferrite. Adding Cr^{3+} ions decreases the lattice volume and the size of the crystallite respectively. FESEM images show non-spherical particles on a largely uniform surface shape with decreasing grain size on doping Cr^{3+} . The FTIR pattern supports the XRD patterns for spinel ferrite.

Keywords
Nanoferrites, Cr^{3+} substitute, XRD, FESEM, FTIR.

Article information
Manuscript received: September 6, 2023; Accepted: October 13, 2023
DOI https://doi.org/10.3126/bibechana.v20i3.58411

1 Introduction

The investigation of nano-scale magnetic materials and their properties is currently a highly active area of research due to their unique and captivating attributes. These properties often differ from those of larger bulk substances due to their high surface-to-volume ratio [1–3]. Nanoscale particles, with applications in diverse fields such as bioprocessing, color imaging, memory storage devices, ferrofluids, and magnetic refrigeration, have gained significant attention [4–6]. Ferrites can be categorized as either soft or hard based on their magnetization and demagnetization characteristics [7]. These ferrites encompass four crystal chemistry categories: spinel ferrites, garnet ferrites, magnetoplumbite ferrites, and orthorhombic ferrites [8–10]. Among these, spinel ferrites, denoted by the chemical formula MFe2O4 where M represents a divalent metal cation, have emerged as the most extensively researched due to their remarkable optical and magnetic properties [11–13]. Spinel ferrites find applications in sensors, electromagnets, optoelectronic components, high-frequency devices, and more [14, 15]. They exhibit exceptional attributes such as higher resistivity values, magneti-

zation, permeability, and lower eddy current losses [16]. The distinct properties of spinel ferrites can be influenced by factors such as sintering temperature, preparation methods, choice of dopant ions, particle size, and agglomeration [17–19]. Extensive studies have focused on utilizing divalent and trivalent metal ions to enhance the electrical, optical, and magnetic characteristics of ferrites. Notable substitutions, like replacing Fe3+ with Cr^{3+} in cobalt ferrite, have been explored without altering the spinel structure [20]. While there has been considerable exploration of divalent ion replacements, trivalent cations have not been as extensively studied as potential substitutes in spinel materials [21].

The most notable cobalt and spinel ferrite compound is $CoFe_2O_4$, which possesses a combination of advantageous features suitable for high-density magnetic recording applications. These include low cost, high coercivity, mechanical hardness, and chemical stability, making it an ideal choice [22]. Within this structure, half of the Fe^{3+} ions occupy tetrahedral sites, while the remaining half occupies octahedral sites, resulting in an inverse spinel configuration [23, 24]. By substituting different metal ions into the cobalt lattice, ferrite materials with novel properties are generated. The characteristics of these materials are significantly influenced by factors such as preparation conditions, the quantity and type of substituent [17, 25–28].

When non-magnetic copper is introduced as a substitution into the cobalt ferrite lattice, it is expected to induce distortions in the spinel structure [29–32]. The addition of copper results in an intriguing distribution of cations across the interstitial sites A and B within the cobalt ferrite lattice [33]. Cu^{2+} is a Jahn-Teller ion with degenerate orbitals, exhibiting high electrical conductivity in its ground state [34]. The introduction of Cu^{2+} ions can induce crystal distortions [35]. Reports suggest that the positioning of Cu^{2+} ions at A and B sites influences the extent of crystal distortion they cause [36–38].

Our recent research has investigated the impact of Cr^{3+} substitution in cobalt-copper ferrite compositions ($Co_{0.7}Cu_{0.3}Fe_{2-x}Cr_xO_4$) and $Cu_{0.7}Co_{0.3}Fe_{2-x}Cr_xO_4$) [2, 39–42]. It was observed that the inclusion of Cr^{3+}ions in the cobalt ferrite lattice leads to a decrease in saturation magnetization due to the lower magnetic moment of Cr^{3+} ions compared to Fe^{3+} ions. Additionally, the electrical resistivity increased as the concentration of Cr^{3+} ions rose. This phenomenon can be attributed to the single stable oxidation state of chromium ions, which reduces the efficiency of conduction involving Fe^{2+} and Fe^{3+} ions, resulting in higher resistivity. Various techniques have been employed to produce cobalt-copper ferrite nanoparticles [43, 44]. Among these, the sol-gel process, known for generating heterogeneous and crystalline nanoparticles, stands out as a chemical method capable of effectively producing ferrite nanoparticles [45]. This process involves hydrolyzing and condensing metal precursors to form a three-dimensional inorganic system. Metal precursors are utilized in this low-temperature synthesis process [46]. This study aims to investigate the structural and morphological properties of Co-Cu ($Cu_{0.7}Co_{0.3}Fe_{2-x}Cr_xO_4$) and Cu-Co ($Co_{0.7}Cu_{0.3}Fe_{2-x}Cr_xO_4$) nanoferrites at varying levels of x, specifically x = 0.0, 0.05, 0.1, 0.15, and 0.2. The synthesis of the samples will involve utilizing the sol-gel auto-combustion method. This analysis will employ techniques such as X-ray diffraction (XRD), field emission scanning electron microscopy (FESEM), and Fourier-transform infrared spectroscopy (FT-IR) to examine the resulting structures and morphologies.

2 Experimental Techniques

The initial precursors for the synthesized materials include cobalt, copper, iron, chromium nitrates, and citric acid, all obtained from Sigma Aldrich with a purity of 98%. A chelating agent, citric acid, was used to form complexes with the metal nitrates. To create the citric acid solution, the nitrates were mixed with citric acid in a 1:1 ratio. The resulting mixture was stirred magnetically at temperatures between 80 and 90^0 Celsius for a duration of 10-12 hours, leading to the formation of a viscous gel. This gel was then subjected to drying at 1000 degrees Celsius for 6 hours. The product was decomposed using spontaneous self-ignition and subsequently powdered using a mortar and pestle. The powdered material was annealed at 1100^0C for 4 hours to eliminate impurities.

Phase identification of the Cr^{3+} substituted Co-Cu ($Co_{0.7}Cu_{0.3}Fe_{2-x}Cr_xO_4$) and Cu-Co ($Cu_{0.7}Co_{0.3}Fe_{2-x}Cr_xO_4$) nanoferrites was carried out using X-ray diffraction (XRD) with a Cu-K x-ray radiation source. X'PERT PRO software was employed to analyze the X-ray diffraction patterns within the range of 20 to 80^0 diffraction angles. The surface morphology and elemental distribution of the synthesized samples were studied using FESEM (Field Emission Scanning Electron Microscopy) models Quanta 250 and FEI D9393. Furthermore, different vibrational modes in the prepared samples were determined using FTIR (Fourier-Transform Infrared) spectrometers, 400 FTIR, and FIR (Far-Infrared).

Force constants calculations

$$v_1^2 = \frac{1}{2\pi c}\sqrt{\frac{K}{\mu}} \tag{1}$$

where $\mu = \frac{\mu_1\mu_2}{\mu_1+\mu_2}$ for two atoms systems. Tetra-

hedral and Octahedral Force constants K_T and K_O are directly proportional to the vibration frequency and molecular weights (μ_A, μ_B) by the following relations as suggested by Waldron [47]:

$$K_T = 4\pi^2 c^2 \mu_A v_1^2 \quad (2)$$

$$K_0 = 4\pi^2 c^2 \mu_B v_2^2 \quad (3)$$

Cation distribution data was used to estimate the molecular weights of A- and B-sites. The molecular weights (μ_A and μ_B) and force constants (K_T and K_O) are directly proportional to each other.

The values of tetrahedral and octahedral radii (r_A and r_B) can be calculated using the equations given below:
$r_A = Cobalt\ content \times r_{Co} + Copper\ content \times r_{Cu} + Iron\ content \times r_{Fe}$
and $r_B = \frac{1}{2}[Cromium\ content \times r_{Cr} + Iron\ content \times r_{Fe}]$

The theoretical lattice constants have also been estimated using the following formulae by proposing the cationic distribution of metal ions in the spinel lattice.

$$r_A = (u - \frac{1}{4})a_{th}\sqrt{3} - R_0 \quad (4)$$

$$r_B = (\frac{5}{8} - u)a_{th} - R_0 \quad (5)$$

$$a_{th} = \frac{8}{3\sqrt{3}}\left[(r_A + R_0) + \sqrt{3}(r_A + R_0)\right] \quad (6)$$

Where, r_A and r_B are radii of tetrahedral and octahedral sites respectively. a_{th} is theoretical lattice constants. R_o is the radius of the oxygen ion. u is the oxygen positional parameter. For the fcc structure, R_o is 0.375. In the Co-Cu ferrite system, the radii of Cr^{3+} and Co^{2+} ions are greater than the space occupied by the oxygen ions. This will cause distortion in the cubic lattice and therefore the oxygen parameter may differ from its usual value of 3/8 [48].

3 Results and Discussion

3.1 XRD Study

The X-ray diffraction (XRD) patterns of Cr^{3+} substituted Co-Cu ($Co_{0.7}Cu_{0.3}Fe_{2-x}Cr_xO_4$) and Cu-Co ($Cu_{0.7}Co_{0.3}Fe_{2-x}Cr_xO_4$) nanoferrites, where x = 0.0, 0.05, 0.1, 0.15, 0.2, and 0.25, are presented in Figure 1 (a) and (b). These patterns reveal the presence of a single-phase spinel structure [**?**,35,49], specifically related to the Fd3m space group with a card number of 22-1086 [50]. The XRD patterns exhibit distinct and well-defined peaks in the (111), (220), (311), (222), (400), (422), (511), (440), (620), and (533) planes, indicating a high degree of crystallinity that aligns closely with existing literature [28,51,52].

The values in Table 1 exhibit a gradual decrease due to the substitution of Cr^{3+}ions. For Co-Cu nanoferrites, the lattice parameter reduces from 8.4498 Å to 8.4321 Å, while for Cu-Co nanoferrites, it decreases from 8.4441 Å to 8.4099 Å. This decrease is attributed to the larger ionic radii of Fe^{3+} ions (0.645) compared to Cr^{3+} ions (0.615) [53].

3.2 FESEM analysis

Utilizing field effect scanning electron microscopy (FESEM), the characterization of shape and grain size in Cr^{3+} substituted Co-Cu ($Co_{0.7}Cu_{0.3}Fe_{2-x}Cr_xO_4$) and Cu-Co ($Cu_{0.7}Co_{0.3}Fe_{2-x}Cr_xO_4$) nanoferrites, where x = 0.0, 0.05, 0.1, 0.15, 0.2, and 0.25, has been conducted. The FESEM micrographs of the synthesized nanoferrites are depicted in Figures 3 (a) and (b). Extensive research has been undertaken by various investigators to gain a deeper understanding of fine-grain morphology [54,55]. The FESEM micrographs reveal agglomerated, spherical, refined, and densely packed magnetic nanoparticles with an average grain size ranging from 50 to 100 nm. Remarkably, this study corroborates the findings by establishing a robust correlation between the grain size deduced from the observed FESEM micrograph analysis and the crystallite size determined from the XRD diffraction patterns of the synthesized samples [53].

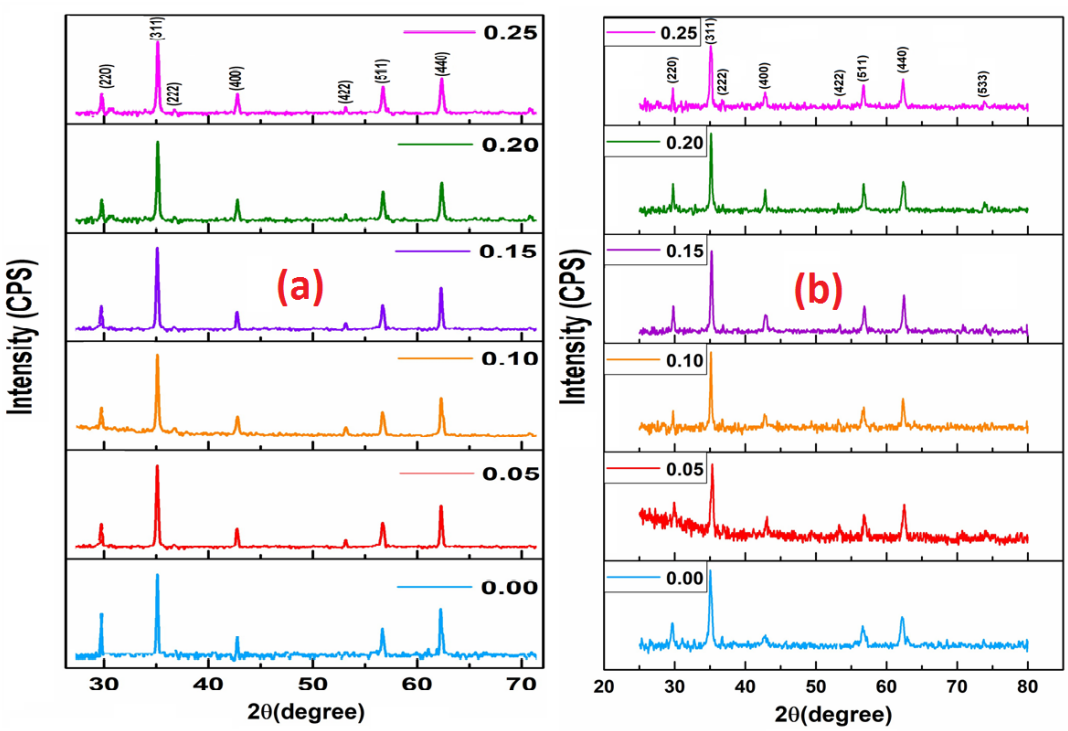

Figure 1: (a) and (b): XRD images of Cr^{3+} doped Co-Cu and Cu-Co nano ferrite.

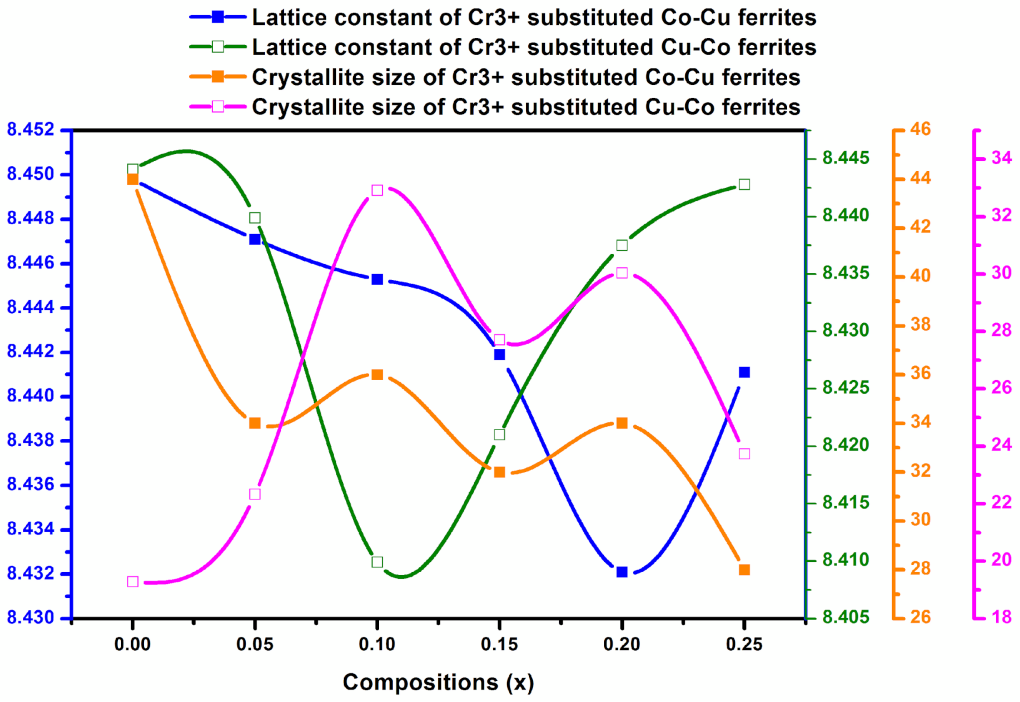

Figure 2: Lattice constant and crystallite size vs. composition of the Cr^{3+} substituted Co-Cu and Cu-Co nano ferrite.

Table 1: Experimental values for different concentrations of the samples

Composition (x)	Cr^{3+} substituted Co-Cu		Cr^{3+} substituted Cu-Co	
	Lattice Constant (Å)	Crystallite size (nm)	Lattice Constant (Å)	Crystallite size (nm)
$x = 0.0$	8.4498	44	8.4441	19.28
$x = 0.05$	8.4471	34	8.4399	22.33
$x = 0.1$	8.4453	36	8.4099	32.92
$x = 0.15$	8.4419	32	8.4210	27.71
$x = 0.2$	8.4321	34	8.4375	30.04
$x = 0.25$	8.4411	28	8.4428	23.74

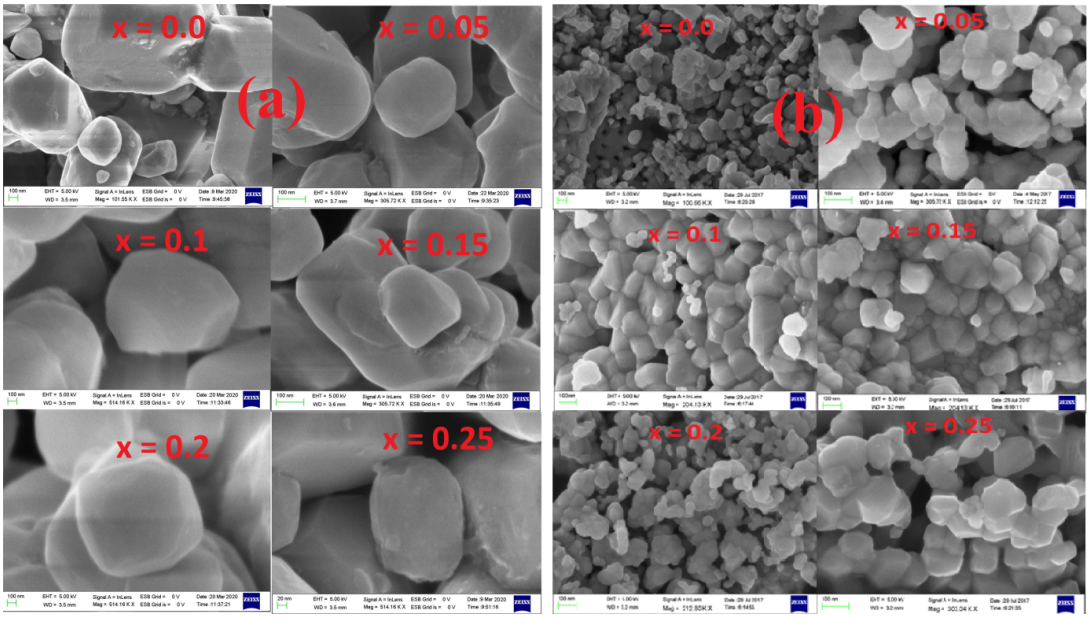

Figure 3: (a) and (b): FESEM images of Cr^{3+} substituted Co-Cu and Cu-Co nanoferrite.

The substitution flexibility within available lattice sites diminishes as particle growth occurs, particularly when the chosen substituted element exhibits a pronounced affinity for a specific site. This results in a more controlled nucleation process and particle size. It is widely recognized that cobalt and chromium ions exhibit a strong preference for occupying octahedral sites within the lattice structure [56].

3.3 FTIR analysis

FTIR spectroscopy is employed to analyze vibrational modes, investigate structural stability, and assess cation distribution within interstitial sites. Figures 4 (a) and (b) display the typical FTIR spectra of Cr^{3+} substituted Co-Cu ($Co_{0.7}Cu_{0.3}Fe_{2-x}Cr_xO_4$) and Cu-Co ($Cu_{0.7}Co_{0.3}Fe_{2-x}Cr_xO_4$) nano ferrites, where x = 0.0, 0.05, 0.1, 0.15, 0.2, and 0.25. These spectra were obtained using the samples prepared by the sol-gel method, with samples sintered at 1100^0C for 4 hours. The transmittance spectra were executed within wavenumbers of 350 to 800 cm^{-1} at room temperature. Notably, below 800 cm^{-1}, the presence of two prominent absorption bands affirms the formation of a spinel structure in the synthesized ferrites [57]. Furthermore, these spectra offer insights into the functional groups present in the ferrite compositions. Two distinct vibrational bands, labeled v_1 and v_2, arise due to stretching vibrations occurring at both octahedral and tetrahedral sites. The vibrational band v1 corresponds to the stretching vibrations of M^{3+}-O2 (M^{3+} = Cr^{3+} and Fe^{3+}) bonds in octahedral sites. In contrast, the vibrational band v2 can be attributed to the intrinsic vibrations of M^{2+}-O2 (M^{2+} = Co^{2+}, Cu^{2+}, and Fe^{2+}) bonds in tetrahedral sites. This distinction arises due to the shorter Fe-O bond length (0.189 nm) in tetrahedral sites compared to octahedral sites (0.199 nm). Consequently, all ferrites exhibit these

two distinct bands, influenced by the closer coupling of Fe^{3+} ions at A sites rather than B sites. The positions of these vibrational bands alter as the Cr^{3+} doping density increases. This phenomenon is due to the substitution of larger Fe^{3+} ions by smaller Cr^{3+} ions, resulting in a change in site radius. A notable relationship between site radius and fundamental frequency is observed, where a decrease in site radius leads to an increase in the fundamental frequency [18]. The presence of substituted Cr^{3+} ions disrupts the (Fe^{3+} - O2) connections and perturbs the lattice structure, leading to a broadening of the high-frequency absorption band [58]. Table 2 provides the A and B band positions for samples at different levels of Cr^{3+} doping.

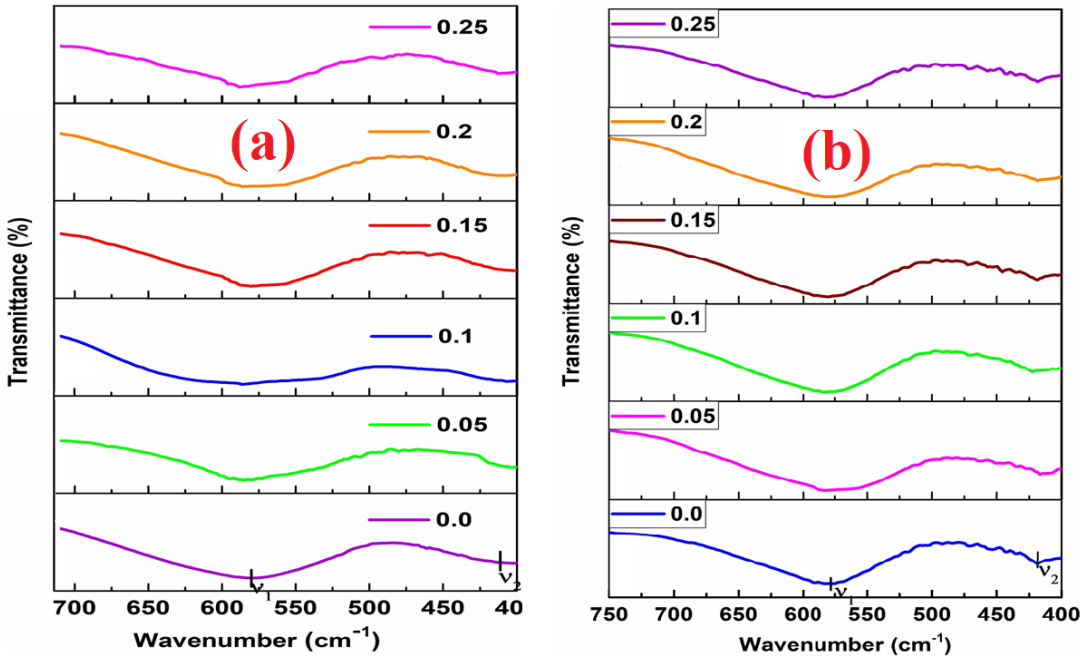

Figure 4: (a) and (b): FTIR spectra of Cr^{3+}substituted Co-Cu and Cu-Co nanoferrite.

Table 2: Tetrahedral (υ_1) and Octahedral (υ_2) absorption bands Fe^{3+} - O^{2-} bond force constants and of Cr^{3+} substituted Co-Cu and Cu-Co nanoferrite

Ferrite composition	Cr^{3+} substituted Co-Cu				Cr^{3+} substituted Cu-Co			
	υ_1 (cm^{-1})	υ_2 (cm^{-1})	Fe^{3+}-O^{2-} bond force constant (10^5 dyne/cm)		υ_1 (cm^{-1})	υ_2 (cm^{-1})	Fe^{3+}-O^{2-} bond force constant (10^5 dyne/cm)	
			K_T	K_O			K_T	K_O
x = 0.0	580.573	402.122	2.5791	1.3614	580.574	418.553	2.5701	1.3604
x = 0.05	584.431	404.051	2.5292	1.3675	582.502	420.624	2.6292	1.3675
x = 0.1	586.360	406.980	2.4717	1.3733	584.431	422.411	2.4717	1.3703
x = 0.15	582.502	402.122	2.4799	1.3796	580.164	418.239	2.4709	1.3706
x = 0.2	586.360	410.837	2.4554	1.3980	580.844	418.695	2.4604	1.3800
x = 0.25	588.288	412.766	2.4472	1.4041	580.175	418.508	2.4462	1.4031

4 Conclusion

The cost-effective sol-gel auto-combustion technique was successfully utilized to synthesize single-phase, well-crystallized ultrafine crystals of Cr^{3+} substituted Co-Cu ($Co_{0.7}Cu_{0.3}Fe_{2-x}Cr_xO_4$) and Cu-Co ($Cu_{0.7}Co_{0.3}Fe_{2-x}Cr_xO_4$) nanoferrites, where x = 0.0, 0.05, 0.1, 0.15, 0.2, and 0.25. The resulting ferrite samples exhibit a face-centered cubic structure characterized by the Fd-3m space group.

The crystallite size of Cr^{3+} substituted Co-Cu is larger than that for Cu-Co. Notably, the cation distribution analysis indicates a preference for octahedral B-sites for Co^{2+}, Cu^{2+}, and Cr^{3+} ions within the lattice. The force constant is directly proportional to the atomic weights of the constituents in the respective lattice sites. The data reveals that the Cu-Co ferrite substituted with Cr is slightly more efficient than its counterpart.

Data Declaration

Data can be obtained from the corresponding author on request.

Competing Interest

The authors declare they have no competing interests.

References

[1] S. Akter, M. N. I. Khan, F. Ferdous, H. N. Das, and I. M. Syed. Analysis of the influence of trivalent cr^{3+} doping on the structural and electromagnetic properties of $cu_{0.5}mg_{0.5}cr_xfe_{2-x}o_4$ nanoferrites. *AIP Adv.*, 12:95015, 2022.

[2] H. Rao Daruvuri, K. Chandu, N. Murali, D. Parajuli, Y. Mulushoa S, and M. P. Dasari. Effect on structural, dc electrical resistivity, and magnetic properties by the substitution of zn^{2+} on co-cu nano ferrite. *Inorg. Chem. Commun.*, 143:109794, 2022.

[3] R. Vijaya Bharathi, M. K. Raju, S. Uppugalla, V. Raghavendra, D. Parajuli, B. Suryanarayana, S. Yonatan Mulushoa, N. Murali, and K. Samatha. Cu^{2+} substituted mg-co ferrite has improved dc electrical resistivity and magnetic properties. *Inorg. Chem. Commun.*, 149:110452, 2023.

[4] R. K. Panda, R. Muduli, G. Jayarao, D. Sanyal, and D. Behera. Effect of cr^{3+} substitution on electric and magnetic properties of cobalt ferrite nanoparticles. *J. Alloys Compd.*, 669:19, 2016.

[5] A. A. Al-Juaid and M. A. Gabal. Effects of co-substitution of al^{3+} and cr^{3+} on structural and magnetic properties of nano-crystalline $cofe_2o_4$ synthesized by the sucrose technique. *J. Mater. Res. Technol.*, 14:10, 2021.

[6] K. L. V. Nagasree, B. Suryanarayana, V. Raghavendra, S. Uppugalla, T. Wegayehu Mammo, D. Kavyasri, N. Murali, M. K. Raju, D. Parajuli, and K. Samatha. Influence of mg^{2+} and ce^{3+} substituted on synthesis, structural, morphological, electrical, and magnetic properties of cobalt nano ferrites. *Inorg. Chem. Commun.*, 149:110405, 2023.

[7] B. P. Jacob, S. Thankachan, S. Xavier, and E. M. Mohammed. Effect of tb^{3+} substitution on structural, electrical and magnetic properties of sol–gel synthesized nanocrystalline nickel ferrite. *J. Alloys Compd.*, 578:314, 2013.

[8] B. P. Jacob, S. Thankachan, S. Xavier, and E. M. Mohammed. Dielectric behavior and ac conductivity of tb^{3+} doped $ni_{0.4}zn_{0.6}fe_2o_4$ nanoparticles. *J. Alloys Compd.*, 541:29, 2012.

[9] I. Lisser, M. Belaiche, M. Elansary, Y. Mouhib, C. Ahmani Ferdi, and M. Tabyaoui. Magnetic and structural properties of novel-coated multi-doped ni–co ferrite nanomaterial: Experimental and theoretical investigations. *J. Mater. Res.*, 38:1669, 2023.

[10] C. Murugesan, B. Sathyamoorthy, and G. Chandrasekaran. Structural, dielectric and magnetic properties of gd substituted manganese ferrite nanoparticles. *Phys. Scr.*, 90:085809, 2015.

[11] B. Suryanarayana, K. Ramanjaneyulu, V. Raghavendra, N. Murali, D. Parajuli, S. Yonatan Mulushoa, P. Choppara, P. A. Rao, Y. Ramakrishna, and K. Chandramouli. Effect of sm3+ substitution on dc electrical resistivity and magnetic properties of ni–co ferrites. *J. Indian Chem. Soc.*, 99:100623, 2022.

[12] D. Parajuli, P. Taddesse, N. Murali, and K. Samatha. Study of structural, electromagnetic and dielectric properties of cadmium substituted ni–zn nanosized ferrites. *J. Indian Chem. Soc.*, 99:100380, 2022.

[13] D. Parajuli, P. Taddesse, N. Murali, and K. Samatha. Correlation between the structural, magnetic, and dc resistivity properties of co0.5m0.5-xcuxfe2o4 (m = mg, and zn) nano ferrites. *Appl. Phys. A Mater. Sci. Process.*, 128:1, 2022.

[14] C. Komali, N. Murali, K. Rajkumar, A. Ramakrishna, S. Yonatan Mulushoa, D. Parajuli, P. N. V. V. L. Pramila Rani, S. Ampolu, K. Chandra Mouli, and Y. Ramakrishna. Probing the dc electrical resistivity and magnetic properties of mixed metal oxides cr3+ substituted mg–zn ferrites. *Chem. Pap.*, 77:109, 2023.

[15] D. Parajuli, V. Raghavendra, B. Suryanarayana, P. A. Rao, N. Murali, P. V. S. K. P. Varma, R. G. Prasad, Y. Ramakrishna, and K. Chandramouli. Corrigendum to 'cadmium substitution effect on structural, electrical and magnetic properties of ni-zn nano ferrites'. *Results Phys.*, 23:103947, 2021.

[16] C. Rambabu et al. Effect of la3+and ni2+ substitution on sr1-xlaxfe12-yniyo19 hexaferrite structural, magnetic, and dielectric properties. *Mater. Sci. Eng. B*, 289:116257, 2023.

[17] D. Parajuli, N. Murali, and K. Samatha. Structural, morphological, and magnetic properties of nickel substituted cobalt zinc nanoferrites at different sintering temperature. *J. Nepal Phys. Soc.*, 7:24, 2021.

[18] P. P. Hankare, V. T. Vader, N. M. Patil, S. D. Jadhav, U. B. Sankpal, M. R. Kadam, B. K. Chougule, and N. S. Gajbhiye. Synthesis, characterization and studies on magnetic and electrical properties of mg ferrite with cr substitution. *Mater. Chem. Phys.*, 113:233, 2009.

[19] Y. Lu, T. Zhang, Y. Liu, and G. Luo. Preparation of fepo4 nano-particles by coupling fast precipitation in membrane dispersion microcontactor and hydrothermal treatment. *Chem. Eng. J.*, 210:18, 2012.

[20] D. A. Vinnik et al. Electromagnetic properties of zinc–nickel ferrites in the frequency range of 0.05–10 ghz. *Mater. Today Chem.*, 20:100460, 2021.

[21] D. A. Vinnik et al. Ni substitution effect on the structure, magnetization, resistivity and permeability of zinc ferrites. *J. Mater. Chem. C*, 9:5425, 2021.

[22] A. V. Trukhanov et al. Evolution of structure and magnetic properties for bafe11.9al0.1o19 hexaferrite in a wide temperature range. *J. Magn. Magn. Mater.*, 426:487, 2017.

[23] M. V. Zdorovets, A. L. Kozlovskiy, D. I. Shlimas, and D. B. Borgekov. Phase transformations in feco – fe2coo4/co3o4-spinel nanostructures as a result of thermal annealing and their practical application. *J. Mater. Sci. Mater. Electron.*, 32:16694, 2021.

[24] K. Dukenbayev et al. Fe3o4 nanoparticles for complex targeted delivery and boron neutron capture therapy. *Nanomater.*, 9:494, 2019.

[25] M. A. Almessiere et al. Correlation between microstructure parameters and anticancer activity of the [mn0.5zn0.5](euxndxfe2-2x)o4 nanoferrites produced by modified sol-gel and ultrasonic methods. *Ceram. Int.*, 46:7346, 2020.

[26] D. Parajuli, V. K. Vagolu, K. Chandramoli, N. Murali, and K. Samatha. Co-precipitation synthesis of zncf nanoparticle and their structure, morphological, and magnetic properties characterization. *J. Nepal Phys. Soc.*, 8:22, 2022.

[27] D. Parajuli, V. K. Vagolu, K. Chandramoli, N. Murali, and K. Samatha. Soft chemical synthesis of nickel-zinc-cobalt-ferrite nanoparticles and their structural, morphological and magnetic study at room temperature. *J. Nepal Phys. Soc.*, 7:14, 2021.

[28] D. Parajuli, V. K. Vagolu, K. Chandramoli, N. Murali, and K. Samatha. Electrical properties of cobalt substituted nzcf and zncf nanoparticles prepared by the soft synthesis method. *J. Nepal Phys. Soc.*, 8:45, 2022.

[29] S. A. Saafan M. A. Darwish D. Zhou A. V. Trukhanov S. V. Trukhanov R. E. El-Shater, H. El Shimy and F. Fakhry. Synthesis, characterization, and magnetic properties of mn nanoferrites. *J. Alloys Compd.*, 928:166954, 2022.

[30] D. Parajuli and K. Samatha. Structural analysis of cu substituted ni-zn in ni-zn ferrite. *BIBECHANA*, 18:128, 2021.

[31] D. Parajuli and K. Samatha. Correlation between the magnetic and dc resistivity studies of cu substituted ni and zn in ni-zn ferrites. *BIBECHANA*, 19:61, 2022.

[32] D. Parajuli and K. Samatha. Morphological analysis of cu substituted ni-zn in ni-zn ferrites. *BIBECHANA*, 18:80, 2021.

[33] A. L. Kozlovskiy and M. V. Zdorovets. Effect of doping of ce4+/3+ on optical, strength and shielding properties of (0.5-x)teo2-0.25moo-0.25bi2o3-xceo2 glasses. *Mater. Chem. Phys.*, 263:124444, 2021.

[34] M. A. Darwish M. U. Khandaker A. Sulieman N. Tamam S. V. Trukhanov A. V. Trukhanov M. A. El-Ghobashy, H. Hashim and M. A. Salem. Eco-friendly nio/polydopamine nanocomposite for efficient removal of dyes from wastewater. *Nanomater.*, 12:1103, 2022.

[35] A. V. Trukhanov S. V. Trukhanov and H. Szymczak. Effect of magnetic fields on magnetic phase separation in anion-deficient manganite la0.70sr0.30mno2.85. *Low Temp. Phys.*, 37:465, 2011.

[36] M. V. Zdorovets M. Ibragimova A. Shumskaya A. A. Rogachev Z. V. Ignatovich A. Kozlovskiy, K. Egizbek and K. Kadyrzhanov. Evaluation of the efficiency of detection and capture of manganese in aqueous solutions of feceox nanocomposites doped with nb2o5. *Sensors*, 20:4851, 2020.

[37] N. V. Pushkarev S. V. Trukhanov, I. O. Troyanchuk and H. Szymczak. Magnetic properties of anion-deficient lal-xba xmno3-x/2 (0 x 0.30) manganites. *J. Exp. Theor. Phys.*, 96:110, 2003.

[38] I. O. Troyanchuk S. V. Trukhanov, M. V. Bushinsky and H. Szymczak. Magnetic ordering in la1-xsrxmno3-x/2 anion-deficient manganites. *J. Exp. Theor. Phys.*, 99:756, 2004.

[39] D. Parajuli N. Murali P. Taddesse S. Y. Mulushoa T. W. Mammo B. Kishore Babu V. Veeraiah P. Himakar, K. Jayadev and K. Samatha. Effect of cu substitution on the structural, magnetic, and dc electrical resistivity response of co0.5mg0.5-xcuxfe2o4 nanoferrites. *Appl. Phys. A Mater. Sci. Process.*, 127:1, 2021.

[40] P. V. S. K. Phanidhar Varma V. Raghavendra K. A. Emmanuel P. Taddesse N. Murali T. Wegayehu Mammo K. Chandramouli, B. Suryanarayana and D. Parajuli. Effect of cr3+ substitution on dc electrical resistivity and magnetic properties of cu0.7co0.3fe2xcrxo4 ferrite nanoparticles prepared by sol-gel auto combustion method. *Results Phys.*, 24:104117, 2021.

[41] D. Parajuli S. Yonatan Mulushoa M. Madhu, A. Venkateswara Rao and N. Murali. Cr3+ substitution influence on structural, magnetic and electrical properties of the ni0.3zn0.5co0.2fe2-xcrxo4 (0.00 x 0.20) nanosized spinel ferrites. *Inorg. Chem. Commun.*, 143:109818, 2022.

[42] M. K. Raju B. Krishan D. Parajuli P. Choppara B. C. Sekhar R. Verma K. M. Batoo G. V. Priya, N. Murali and P. V. L. Narayana. Influence of cr3+ substituted niznco nanoferrites: Structural, magnetic and dc electrical resistivity properties. *Appl. Phys. A Mater. Sci. Process.*, 128:1, 2022.

[43] M. Nawaz A. Manikandan H. S. El Sayed M. A. Almessiere H. Sözeri S. E. Shirsath I. Ercan Y. Slimani, H. Güngüneş and A. Baykal. Magneto-optical and microstructural properties of spinel cubic copper ferrites with li-al co-substitution. *Ceram. Int.*, 44:14242, 2018.

[44] M. A. Almessiere et al. Correlation between composition and electrodynamics properties in nanocomposites based on hard/soft ferrimagnetics with strong exchange coupling. *Nanomater.*, 9:202, 2019.

[45] N. A. Algarou et al. Functional sr0.5ba0.5sm0.02fe11.98o4/x(ni0.8zn0.2fe2o4) hard–soft ferrite nanocomposites: Structure, magnetic and microwave properties. *Nanomater.*, 10:2134, 2020.

[46] Y. Slimani A. Sadaqat A. Baykal A. Manikandan S. V. Trukhanov M. A. Almessiere, N. A. Algarou and A. V. Trukhanov. High-frequency characteristics and spin-canting effects in ni0.5zn0.5fe2o4–ni0.8zn0.2fe2o4 magnetic nanocomposites. *Nanomater.*, 12:665, 2022.

[47] R. D. Waldron. Infrared spectra of ferrites. *Phys. Rev.*, 99:1727, 1955.

[48] J. B. Goodenough and A. L. Loeb. Theory of ionic ordering, crystal distortion, and magnetic exchange due to covalent forces in spinels. *Phys. Rev.*, 98:391, 1955.

[49] N. Murali D. Parajuli, G. C. Kaphle and K. Samatha. Structural identification of cubic aluminum and non-cubic titanium using x-ray diffractometer. *J. Lumbini Eng. Coll.*, 4:62, 2022.

[50] V. Raghavendra B. Suryanarayana K. M. Batoo D. Parajuli, N. Murali and K. Samatha. Investigation of structural, morphological and magnetic study of ni–cu-substituted li0.5fe2.5o4 ferrites. *Appl. Phys. A*, 129:1, 2023.

[51] R. H. Kadam S. T. Alone, S. E. Shirsath and K. M. Jadhav. Chemical synthesis, structural and magnetic properties of nano-structured co–zn–fe–cr ferrite. *J. Alloys Compd.*, 509:5055, 2011.

[52] A. V. Rao A. Ramakrishna Y. M. S D. Parajuli, N. Murali and K. Samatha. Structural, dc electrical resistivity and magnetic investigation of mg, ni, and zn substituted co-cu nano spinel ferrites. *South African J. Chem. Eng.*, 42:106, 2022.

[53] C. Ruttanapun and S. Maensiri. Effects of spin entropy and lattice strain from mixed-trivalent fe3+/cr3+ on the electronic, thermoelectric and optical properties of delafossite cufe1xcrxo2 (x=0.25, 0.5, 0.75). *J. Phys. D. Appl. Phys.*, 48:495103, 2015.

[54] M. Zarrar H. Anwar M. B. Khan Niazi R. Ahmad, I. Hussain Gul and A. Khan. Improved electrical properties of cadmium substituted cobalt ferrites nano-particles for microwave application. *J. Magn. Magn. Mater.*, 405:28, 2016.

[55] U. B. Tumberphale V. V. Jadhav R. S. Mane S. M. Patange S. E. Shirsath A. B. Mugutkar, S. K. Gore and S. S. Jadhav. Role of composition and grain size in controlling the structure sensitive magnetic properties of sm3+ substituted nanocrystalline co-zn ferrites. *J. Rare Earths*, 38:1069, 2020.

[56] A. Goyal S. Jauhar, J. Kaur and S. Singhal. Tuning the properties of cobalt ferrite: A road towards diverse applications. *RSC Adv.*, 6:97694, 2016.

[57] A. S. Nawara N. I. Abu-Elsaad and S. A. Mazen. Synthesis, structural characterization, and magnetic properties of ni–zn nanoferrites substituted with different metal ions (mn2+, co2+, and cu2+). *J. Phys. Chem. Solids*, 146:109620, 2020.

[58] M. A. Abdo S. F. Mansour and S. M. Alwan. The role of cr3+ ions substitution on structural, magnetic and dielectric modulus of manganese zinc nanoferrites. *Ceram. Int.*, 44:8035, 2018.